Accuracy of alloy partial densities of states as determined by valence-band photoelectron diffraction

A. Stuck,* J. Osterwalder,† T. Greber,† and L. Schlapbach
Institut de Physique, Université de Fribourg, CH-1700 Fribourg, Switzerland

R. C. Albers
Los Alamos National Laboratory, Los Alamos, New Mexico 87545

M. Alouani
Department of Physics, Ohio State University, Columbus, Ohio 43210
(Received 31 May 1994; revised manuscript received 1 November 1994)

We present a systematic study of a recently proposed deconvolution of valence-band spectra of alloys into partial densities of states by x-ray photoelectron diffraction. The deconvolution is performed along the [111], [112], [113], and [114] directions of a $AuCu_3$ (001) crystal. As expected, there are only small variations in the partial densities of states as a function of direction, except for the [111] direction. The mathematical assumptions and experimental limitations of the method are discussed in detail.

I. INTRODUCTION

Valence-band (VB) partial densities of states (PDOS) are an essential ingredient that is needed to provide a basic understanding of the physical and chemical properties of alloys. Among the few experimental techniques that can, in principle, measure PDOS are x-ray emission and resonant photoemission, the latter usually exploiting Cooper minima or Fano resonances in the energy dependence of photoelectric cross sections.[1–3] Stuck *et al.*[4] have recently shown that this same sort of information can also be obtained from the angular dependence of photoelectric cross sections in photoelectron diffraction (PD). The basic idea is to use the different PD patterns of the constituents making up the alloy to sort out their contributions to the total DOS. This method has been applied to $AuCu_3$,[4] $LaNi_5$,[5] and very recently to TiO_2.[6] It should also, in principle, be applicable to any ordered alloy or compound whose atoms sit on crystallographically inequivalent sites. Moreover, like most photoemission experiments, it probes both surface and more bulklike electronic-structure information.

In this work we establish the accuracy of this method and its fundamental limitations. We discuss the theoretical assumptions in detail and verify them with VB spectra of $AuCu_3$ (001) measured along the [111], [112], [113], and [114] directions under various experimental conditions.

The basis of the technique depends on the very pronounced anisotropies of the photoelectrons excited from single crystal surfaces; these anisotropies are due to photoemission final-state scattering and diffraction. At a typical high kinetic energy of 1 keV, these diffraction patterns have been found to depend only weakly on the angular momentum and kinetic energy of the photoelectrons. Instead, they are dominated by the local crystalline structure around the emitting atom.[7–9] For example, in Ir the angular-momentum dependence only slightly modifies the anisotropy[10] while leaving the structure of the pattern basically unchanged. Surprisingly, as was shown by Osterwalder *et al.*[8] for Al (001), this same situation is even true in the case of very delocalized VB electrons. In the case of alloys and compounds, the observed differences in diffraction patterns of different constituents, therefore, mainly reflect different local environments.

Because these different diffraction patterns can be measured very accurately for shallow core levels that are emitted with kinetic energies close to those of the VB electrons, they can serve as fingerprints for the emission pattern of the respective elements within the valence band and can be used to decompose the VB emission of ordered alloys and compounds into the contributions from each element. This method, of which we have given a brief account elsewhere,[4] is independent of parameters such as the photon intensity, the instrumental response, and the photoelectric cross sections of each element. Strictly speaking, for each element of the compound, this approach provides partial electron-distribution curves (PEDC), which are equivalent to the PDOS's weighted by their respective photoelectric cross sections. Additional satellite structure may also be present for materials with unfilled shells. The ratios of the VB to core-level cross sections for each element are simultaneously determined by the procedures used in this method.

II. EXPERIMENTAL DETAILS

The experiments were done with a VG ESCALAB MK II spectrometer that had a typical working pressure of 5×10^{-11} mbar in which the samples usually remained clean for several days. A high-precision manipulator allowed us to rotate the crystals in any desired direction with an accuracy of about 0.2°. In a given direction the

photoelectrons excited by unmonochromatized Mg $K\alpha$ radiation were measured with a full-cone angular resolution of about 1°. In one experiment the angular resolution was varied between 1° and 2.2°. To measure the PD curves, a photoelectron spectrum was recorded at each angular setting and analyzed automatically with a linear background subtracted from the signal. To record the azimuthal diffraction patterns, the samples were rotated in 2° steps around the crystal normal. A series of azimuthal scans were combined to create two-dimensional diffraction maps by first fixing the polar angle at $\theta_{\max}=78°$ and then reducing it by 2° after each full azimuthal rotation. The azimuthal step size was increased at lower angles to give an almost uniform sampling density over the hemisphere.[7] About 4000 angular settings were scanned in this way.

All samples were oriented to better than 1° with x-ray Laue diffraction. They were cleaned *in situ* by repeated cycles of Ar^+ sputtering and subsequent annealing. The crystalline order of the surface was verified by low-energy electron diffraction. During the measurements, less than 10% of a monolayer of oxygen and carbon were collected on any of the three different $AuCu_3$ (001) crystals that were used. All the points shown in the figures were measured and no symmetry operation of any kind was performed on the data. In all the experimental energy spectra discussed below, before the deconvolution, a linear background was subtracted and the spectra were corrected for Mg $K\alpha$ satellites. Other background-subtraction procedures were also used with no significant change in the form of the PEDC's.

III. THEORY

Photoemission experiments send photons into a material and excite electrons from an initial state $|i\rangle$ into a final state $|f\rangle$. If the final-state kinetic energy E_f of the excited electrons is high enough, they can escape from the surface of the material with a probability of $T(E_f,\mathbf{k}_f)$, and can then be detected in the direction of the final-state wave vector $\mathbf{k}_f$. Therefore, the contribution $J_i(E_f)$ of electrons in the initial state $|i\rangle$ to the measured photoemission current is given by[11]

$$J_i(E_f)\sim|M_{fi}|^2T(E_f,\mathbf{k}_f)\delta(E_f-E_i-h\nu)\ ,$$
$$M_{fi}=\langle i|\boldsymbol{\varepsilon}\cdot\nabla V_{\text{eff}}|f\rangle\ , \tag{1}$$

where the electron-photon interaction is described by the dipole-operator $\boldsymbol{\varepsilon}\cdot\nabla V_{\text{eff}}$. The unit vector $\boldsymbol{\varepsilon}$ is parallel to the polarization of the incident light and V_{eff} is an effective potential that describes the interaction between a single electron and the solid. Energy conservation is expressed by the δ function and guarantees that the final-state energy E_f is equal to the sum of the initial-state energy E_i and the photon energy $h\nu$.

In solids, the wave functions and potentials can be expanded into contributions from each of the atomic sites $\mathbf{r}_a$; this allows the initial-state wave function with wave vector $\mathbf{k}_i$ and the effective potential to be written as[12]

$$|i\rangle=\sum_a\phi_a^i(\mathbf{r}-\mathbf{r}_a)e^{i\mathbf{k}_i\cdot\mathbf{r}_a}\ ,$$
$$V_{\text{eff}}=\sum_b v_b(\mathbf{r}-\mathbf{r}_b)\ . \tag{2}$$

The precise form of v_b and ϕ_a depends on the physical model used. For example, the v_b could be chosen as a muffin-tin potential and the ϕ_a as Wannier functions. The simplest assumption for the final state is a free-electron wave $|f\rangle=e^{i\mathbf{k}_f\cdot\mathbf{r}}$. The transition matrix element M_{fi} can then be written as

$$M_{fi}=\sum_{a,b}m_{ab}^i e^{i\Delta\mathbf{k}\cdot\mathbf{R}_{ab}}\ ,$$
$$\text{where } \mathbf{R}_{ab}=\frac{\mathbf{r}_a+\mathbf{r}_b}{2} \text{ and } \Delta\mathbf{k}=\mathbf{k}_f-\mathbf{k}_i\ , \tag{3}$$
$$m_{ab}^i=-\langle\phi_a^i(\mathbf{r}-2\delta\mathbf{r}_{ab})|\boldsymbol{\varepsilon}\cdot\nabla v_b(\mathbf{r})|e^{i\mathbf{k}_f\cdot\mathbf{r}}\rangle$$
$$\times e^{-i(\mathbf{k}_f+\mathbf{k}_i)\delta\mathbf{r}_{ab}} \text{ with } \delta\mathbf{r}_{ab}=\frac{\mathbf{r}_a-\mathbf{r}_b}{2}\ .$$

Because the gradient of the effective potential is big near the atomic site b, but essentially zero outside the muffin-tin sphere around atom b, the quantity m_{ab}^i can be interpreted as the contribution of an atom at site a to the photoemission process from site b. If the electrons are emitted from localized states such as core levels, then m_{ab}^i will vanish if the site a is not the same site as b. In photoemission from delocalized states, however, the wave functions extend over many atoms and m_{ab}^i cannot be neglected. Obviously, the sampling of the initial- and final-state wave functions by the effective potential at site b depends on the relative distance and orientation between atom b and atom a. These distances and orientations are affected by vibrations and, therefore, M_{fi} will strongly depend on the sample temperature. Experimentally, one measures the photoelectron intensities averaged over all possible atomic configurations that the solid can have at a given temperature T. If it is assumed that every atom vibrates independently of the other atoms in a harmonic potential and that the mean-square displacement $\langle\Delta u^2\rangle_T$ is the same for every atom, one finds[13]

$$\langle e^{i\Delta\mathbf{k}(\mathbf{r}_1-\mathbf{r}_2)}\rangle_T=e^{-2W}e^{i\Delta\mathbf{k}\cdot(\mathbf{r}_1-\mathbf{r}_2)} \text{ if } \mathbf{r}_1\neq\mathbf{r}_2\ . \tag{4}$$

Here, e^{-2W} is the Debye-Waller factor of the solid and $W=\Delta\mathbf{k}^2\langle\Delta\mathbf{u}^2\rangle_T$. Furthermore, if the wavelength of the electron in the excited state is sufficiently small, i.e., $\mathbf{k}_f$ sufficiently large, and the initial-state wave vector can be restricted to the first Brillouin zone of the solid, then $\Delta\mathbf{k}\sim\mathbf{k}_f$. Clearly, $\langle|m_{ab}^i|^2\rangle_T\sim|m_{ab}^i|^2$ for small vibrations and the photoemission current from initial state $\langle i|$ to final state $|f\rangle$ is approximated by

$$\langle J_i(E_f)\rangle_T\sim(1-e^{-2W})\sum_{a,b}|m_{ab}^i|^2$$
$$+e^{-2W}\sum_{a,b,c,d}\langle m_{ab}^i\overline{m}_{cd}^i\rangle_T e^{i\Delta\mathbf{k}\cdot(\mathbf{R}_{ab}-\mathbf{R}_{cd})}\ . \tag{5}$$

The first term describes incoherent photoemission from

all sites b and does not depend strongly on temperature. Coherent excitations are taken into account by the second term, which in crystals implies the conservation of crystal momentum in the photoemission process and, therefore, describes direct transitions.[14]

For situations involving high temperatures or high kinetic-energy final-state electrons with electron wavelengths comparable to or smaller than the thermal-vibration amplitude, the Debye-Waller factor is small; incoherent emission from different atomic sites dominates the photoelectron spectra. In this x-ray photoemission spectroscopy (XPS) limit the electrons, therefore, behave as if they were emitted independently of each other from different atomic sites. Consequently, the final-state VB diffraction patterns should be very similar to those of localized core levels at comparable kinetic energies. Because $|m_{ab}^{i}|^2$ is independent of $\mathbf{k}_i$, this contribution samples the whole Brillouin zone and will not show any directional dependence of the PEDC's. As mentioned above, Osterwalder *et al.*[8] did indeed observe the same diffraction patterns for Mg $K\alpha$ excited VB electrons ($E=1250$ eV) and Al $2s$ electrons ($E=1180$ eV) in Al(001). The VB spectra mainly reflect the local electronic densities of states around the atomic sites.

At low kinetic energies and low temperatures, however, when the electron wavelength is large compared with the thermal-vibration amplitude, the Debye-Waller factor is close to unity and a strong coherent emission from different atomic sites is expected and observed in UV photoelectron spectroscopy. The VB spectra are then dominated by direct transitions and reflect the band structure of the material. Because of conservation of crystal momentum, this limit gives the possibility of picking up directional PDOS effects due to differences in the underlying band structure in different directions. At moderate temperatures and kinetic energies, the VB spectra will contain both coherent and incoherent contributions.

$AuCu_3$ has a low Debye temperature of 280 K,[15] which corresponds to a Debye-Waller factor of 0.17 for 1.2-keV electrons at room temperature. Under these conditions at least 85–90% of all photoelectrons are emitted incoherently from different atomic sites, since, in addition to thermal disorder, final-state diffraction and instrumental effects further suppress the coherent emission processes.[16] As in the case of elemental Au and Cu,[17,18] only small angular variations are, therefore, expected in the shape of the VB spectra of $AuCu_3$. The total photocurrent at a given energy can, therefore, be approximated by

$$J_{\rm tot}(E_f)\sim\sum_b\left[\sum_{a,i}|m_{ab}^{i}|^2\delta(E_f-E_i-h\nu)\right] . \tag{6}$$

Here the index i indicates that we have to sum over all possible initial states. It is sufficient to sum b only over inequivalent sites of Au and Cu, while a is summed over all atoms in the alloy. The term in the brackets describes the total contribution of all initial states $|i\rangle$ with the correct energy E_i to the photoemission process from site b. Its energy dependence corresponds to $\mu_b^{\rm VB}(E)$, the PEDC of site b, i.e., the photoelectron spectrum one would measure if only electrons from site b could be excited. Another way of writing this term is

$$\begin{aligned}J_b(E_f-h\nu)&=\sum_{a,i}|m_{ab}^{i}|^2\delta(E_f-E_f-h\nu)\\&=\sigma_b^{\rm VB}\frac{\mu_b^{\rm VB}(E_f-h\nu)}{n_b^{\rm VB}} ,\end{aligned} \tag{7}$$

where $\sigma_b^{\rm VB}$ is the average photoelectron cross section of the VB emission from site b, while the total number of VB electrons per site b is given by $n_b^{\rm VB}$. If the matrix elements m_{ab} are only weakly dependent on the particular initial states involved, then they will mostly depend on the number of initial states at a given energy. In other words, the PEDC's will reflect the PDOS of the material.

So far we have neglected final-state diffraction. Electrons emitted from sites with different local surroundings are diffracted differently by the crystal. Therefore, the contribution of two inequivalent atomic sites to the observed photoelectron intensity will also depend on the direction of observation. In $AuCu_3$, the Cu and Au sites are crystallographically inequivalent and the number of photoemitted VB electrons, $I^{\rm VB}(\theta,\phi,E)$, measured at angles θ,ϕ, becomes[4]

$$I^{\rm VB}(\theta,\phi,E)=I_0\sum_{b={\rm Au,Cu}}g_b^{\rm VB}(\theta,\phi,E_f)J_b(E_f) , \tag{8}$$

where the additional factor $g_b^{\rm VB}(\theta,\phi,E_f)$ describes the diffraction of the VB electrons from the bth element in the crystal including their refraction at the surface and the angle-dependent part of the corresponding cross section; I_0 is the photon intensity times the instrumental response.

Equations (7) and (8) show that the angular dependence of the diffraction as well as the photoelectron cross sections are folded into the photoelectron intensity and must, therefore, be factored out to determine the PEDC's. We now show that these quantities can be determined by using the core-electron data.

In a similar way to the valence-band derivation, we find for the energy-integrated core intensities

$$\begin{aligned}S_b^{\rm core}(\theta,\phi)&=\int I_b^{\rm core}(\theta,\phi,E)dE\\&=I_0 g_b^{\rm core}(\theta,\phi,E_f)\sigma_b^{\rm core} .\end{aligned} \tag{9}$$

In the case of Al(001),[8] the relative change in the wavelengths between Mg $K\alpha$ excited Al $2s$ and valence-band electrons is about 4.6%, while it lies between 3% and 3.5% for Au $4f$ and Cu $3p$ $AuCu_3$. Figure 1 shows that such small differences seem to have little effect on the interference patterns. It is, therefore, a good approximation to neglect the energy dependence of $g_b^{\rm VB}(\theta,\phi,E_f)$. Also, the diffraction functions of the core and VB electrons should be approximately equal, i.e., $g_b^{\rm VB}(\theta,\phi)=g_b^{\rm core}(\theta,\phi)$: We can use the measured angular dependence of the core electrons for the valence-band dependence.

A combination of Eqs. (8) and (9) then yields

$$I^{\rm VB}(\theta,\phi,E)=\sum_{b={\rm Au,Cu}}S_b^{\rm core}(\theta,\phi)\frac{\sigma_b^{\rm VB}}{\sigma_b^{\rm core}}\frac{\mu_b^{\rm VB}(E)}{n_b^{\rm VB}} . \tag{10}$$

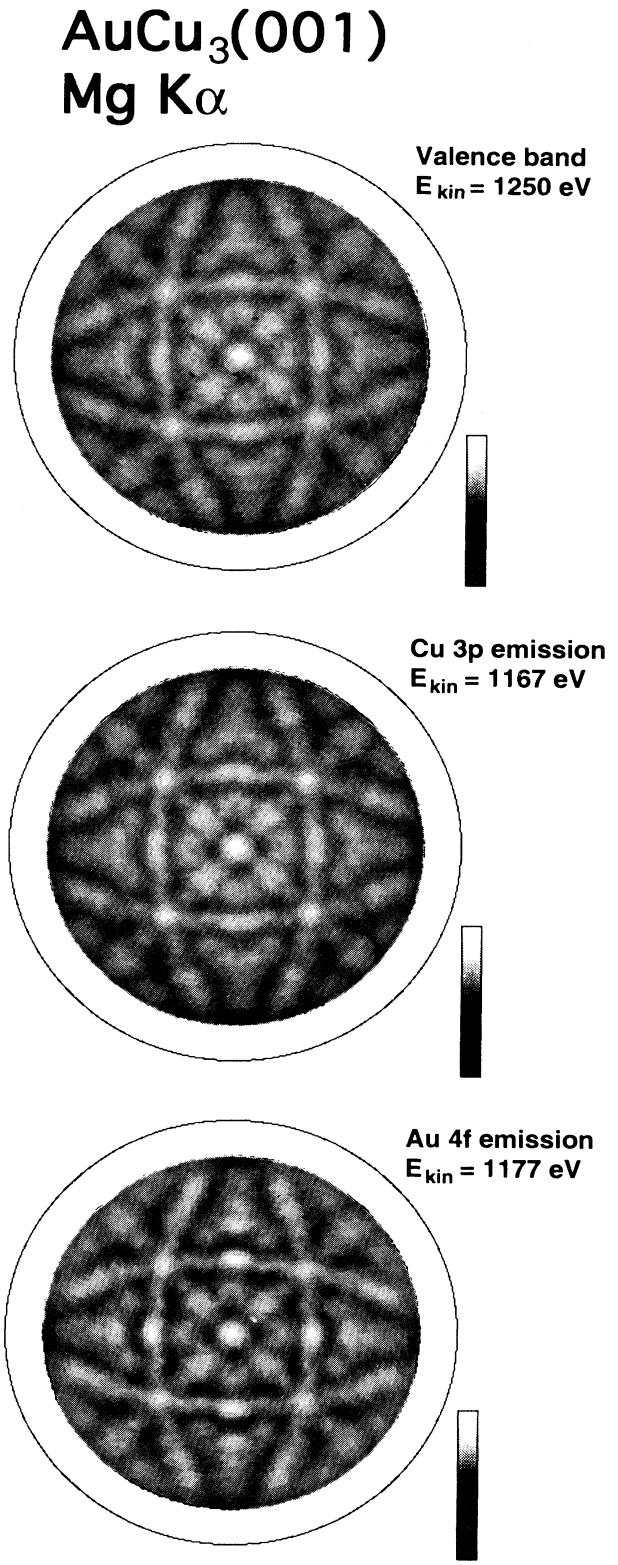

FIG. 1. Two-dimensional VB, Cu 3*p*, and Au 4*f* diffraction maps of $AuCu_3$ (001) in the stereographic projection; the normal is in the center of the images while grazing incidence is marked by the circle. Along the [111], [112], [113], and [114] directions, small diffraction differences between Cu 3*p* and Au 4*f* emission can be identified.

After integrating over all energies within VB emission

$$S^{\mathrm{VB}}(\theta,\phi)=\int I^{\mathrm{VB}}(\theta,\phi,E)dE \ ,$$

we find

$$S^{\mathrm{VB}}(\theta,\phi)=\sum_{b=\mathrm{Au,Cu}} S_b^{\mathrm{core}}(\theta,\phi)\frac{\sigma_b^{\mathrm{VB}}}{\sigma_b^{\mathrm{core}}} \ . \tag{11}$$

Measurements of the energy-integrated core level and VB intensities for at least two different directions, thus, yield a set of linear equations [Eq. (11)], which can be solved for the ratios of the cross sections. Given these two ratios, the angular dependence of the core electrons, and the energy-resolved VB spectra, a second set of linear equations [see Eq. (10)] at each energy can be solved for the PEDC of the two elements.

Any directional dependence of μ_b^{VB} has been neglected so far. As will be shown below, this is not entirely correct, since small variations of the PEDC's as a function of direction are seen experimentally. However, the VB PEDC's change over a much wider angular range than the diffraction pattern. So, if the two directions of analysis are chosen close enough, i.e., within about 10°, the PEDC's in the two directions are equal for all practical purposes. They then correspond to the electron distribution curves of each element one would measure in these two directions, if only the VB electrons of this element would contribute to the signal. Thus, we have a tradeoff between trying to reduce the angular distance between the two directions needed for the deconvolution and the increased numerical instability this creates when we try to solve the coupled equations.

The condition

$$n_b^{\mathrm{VB}}=\int \mu_b^{\mathrm{VB}}(E)dE \tag{12}$$

is implicitly assumed in Eq. (11), and can be used to find the absolute calibration of the PEDC's. As in the case of pure Au and Cu, we find that the photoelectric cross sections for Mg $K\alpha$ excited *s* and *p* VB electrons in $AuCu_3$ are very small and the measurements will, therefore, be strongly dominated by *d*-like electrons. In $AuCu_3$, the number of electrons per unit cell can, therefore, be chosen as $n_{\mathrm{Au}}^{\mathrm{VB}}=10$ electrons/cell and $n_{\mathrm{Cu}}^{\mathrm{VB}}=30$ electrons/cell.

The calculations of the theoretical PEDC's have been done by a self-consistent fully relativistic linear muffin-tin-orbital method.[19] The same algorithm was used for the band-structure calculations of $AuCu_3$, reported by Sohal *et al.*[20] where excellent agreement between theory and experiment was found. The theoretical PEDC's used in this study include cross-section effects that are folded into directional DOS of the *d* electrons along the [111], [112], [113], and [114] directions. These directional DOS $\rho(\mathbf{k},E)$ are calculated from the band structure as follows:[20]

$$\rho(\mathbf{e},E)=\int d\mathbf{K}\sum_i \delta[E-E_i(\mathbf{K})] \ . \tag{13}$$

Here, the vector $\mathbf{K}$ in the integration is restricted to the direction of vector $\mathbf{e}$ and the sum is over all allowed

initial states i of d electrons. Because the directional DOS only contain band-structure information along specific directions and do not sum over the full Brillouin zone (this would give the total DOS), they are equivalent to keeping only the direct (coherent) terms of the PD. They, therefore, exaggerate the Brillouin-zone directional dependence and give an upper limit to the amount of directional dependence that one would expect to see. A more accurate calculation of a specific experiment would sum the coherent (directional DOS) with the incoherent (total DOS) contributions (weighting the contributions by the Debye-Waller factor). As one goes from zero temperature to high temperature, there would be a crossover from a dominant coherent component to the incoherent one. To simulate the broadening due to the Mg $K\alpha$ radiation, the theoretical spectra have been convoluted with a Lorentzian (FWHM = 0.8 eV). This broadening significantly washes out fine structure in the directional-projected DOS and tends to make the projected DOS in all directions more closely resemble the total DOS.

IV. EXPERIMENTAL RESULTS

As can be seen by comparing Figs. 1 and 2, the photoelectron diffraction patterns of $AuCu_3$ at high kinetic energies are essentially a projection of a fcc crystal structure onto the sphere of measurement. As discussed by Naumovic *et al.*,[7] this is due to the strong forward focusing and Bragg scattering (Kikuchi bands) of the electrons at energies above 1 keV. All of the patterns are very similar. A close inspection, however, reveals small differences in the diffraction maps. For example, the maximum of the Au $4f$ emission along [111] in the center of the Y-shaped structures is much narrower than that of the Cu $3p$ emission. The same is true of the structure along the [112] direction. In fact, the Cu $3p$ peaks are split with a local minimum in these two directions while the Au $4f$ emission has a single maximum there. The splitting of the Cu $3p$ diffraction pattern is also observed along the [113] direction and vanishes near the [114] direction. As discussed by Stuck *et al.*[4] for the [111] direction, similar and corresponding variations are measured between the azimuthal scans of two valence-band regions, which have previously been associated with predominantly Au and Cu character.[20,21] These qualitative diffraction differences clearly permit us to associate the VB intensities between 5- and 8-eV binding energy to Au emission and the VB intensities between 0- and 4-eV binding energy to Cu emission. They reflect the different local environments of each element in the ordered phase of $AuCu_3$.[4] Note that at room temperature Au emitters are only present in every other layer,[22,23] which probably explains the differences in the diffraction patterns. Moreover, the Au emitters have 12 Cu nearest neighbors, while there are 8 Cu and 4 Au nearest-neighbor atoms in the case of Cu. Consequently, the local scattering potential is different. Since the contributions from the two elements have directional-dependent weights, the shape of the VB spectra in general depends on the direction of observation. The PEDC's of Au and Cu can be obtained by analyzing these spectral differences separately for each energy measured.

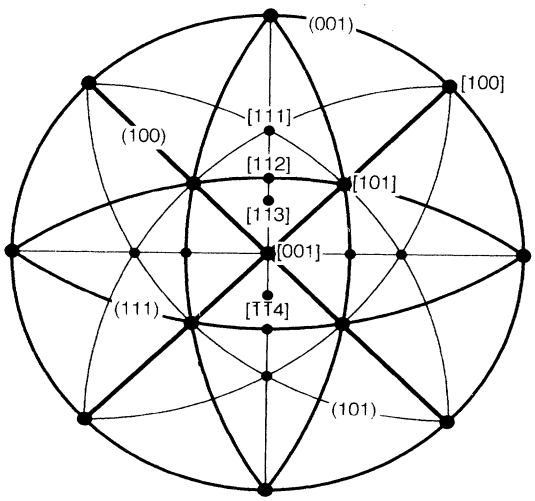

FIG. 2. Stereographic projection of an fcc crystal structure. Low-index crystal planes are shown together with some directions along which forward-scattering peaks are expected.

The ratios of VB to core-level cross sections in $AuCu_3$, as calculated with Eq. (11), are listed in Table I for four sets of measurements along the [111], [112], [113], and [114] directions. The errors associated with these cross-section ratios are large and were estimated to be three times the standard deviation of the data. Polycrystalline Au and Cu were also measured as a reference. The cross-section ratios of these materials were 0.13 ± 0.02 for Au and 0.42 ± 0.04 for Cu.

The experimental PEDC's corresponding to the cross-section ratios from Table I are presented in Figs. 3 and 4. The theoretical curves also shown in these figures are the PEDC's of the d electrons projected onto the same set of directions. It is easily seen from these data that for both Au and Cu the experimental PEDC's along the [112], [113], and [114] directions are very similar to each other. In the case of Au (Fig. 3), the PEDC's are low near the Fermi edge and have a first maximum around 2.6 eV, a local minimum between 4 and 4.5 eV, and a broad flat shoulder between 5 and 7 eV. The first peak at 2.6 eV with a height of 2–2.5 electrons/(eV cell) is systematically higher than the structure between 5 and 7.5 eV with a height of about 1.5–2 electrons/(eV cell). This is different for the [111] direction, where the first peak found at 2.8 eV is about a factor of 2 smaller than the broad structure between 5 and 7 eV. The electron density of the Au PEDC at the minimum between 4 and 4.5 eV

TABLE I. Cross-section ratios for the two elements in $AuCu_3$ obtained from Eq. (11) as a function of direction.

Direction	$\sigma_{\text{Au VB}}/\sigma_{\text{Au }4f}$	$\sigma_{\text{Cu VB}}/\sigma_{\text{Cu }3p}$
[111]	0.095	0.51
[112]	0.099	0.49
[113]	0.077	0.59
[114]	0.086	0.57
average	0.09 ± 0.03	0.54 ± 0.15

does not change. Although the theoretical structures along [111] are slightly broader than the experimental ones, most peak positions and intensities are in good agreement with the measurements along [111]. In particular, theory predicts fewer electrons/(eV cell) around 2.6 eV than between 5 and 7 eV. However, the theoretical Au spectrum along [111] has a local maximum around 2 eV, which is absent in the experimental spectra presented. At higher binding energies, the last peak between 7 to 7.5 eV predicted by theory could not be resolved in the experiment. In contrast to the experimental results, the theoretical Au PEDC's do not change significantly as a function of direction. In particular, the enhancement of the peak around 2.8 eV for the [112], [113], and [114] directions is not predicted.

In Fig. 4, the differences between the Cu PEDC's along [112], [113], and [114] are more pronounced than in the case of Au. All of the Cu PEDC's are dominated by a single peak at around 3 eV, which appears slightly shifted towards lower binding energy in the [111] direction. In addition, along the [112], [113], and [114] directions a broad shoulder appears between 5 and 7.5 eV. This structure is completely lacking in the data along [111]. So, the electrons in this energy region are distributed differently among the two elements for different directions. In the [112], [113], and [114] directions, some electrons between 5 and 7.5 eV are attributed to Cu, which effectively lowers the Au PEDC in this energy range. In contrast, essentially all the electrons above 5 eV are attributed to Au along the [111] direction, which explains the dominance of the Au PEDC in this region. Theory predicts a slightly split peak with a first maximum at 1.8 eV, a second peak at 2.8 eV, and a low shoulder above 4 eV for the Cu PEDC along [111]. Experimentally the splitting is not resolved. The predicted densities, the central peak position, and the general shape of the Cu PEDC are

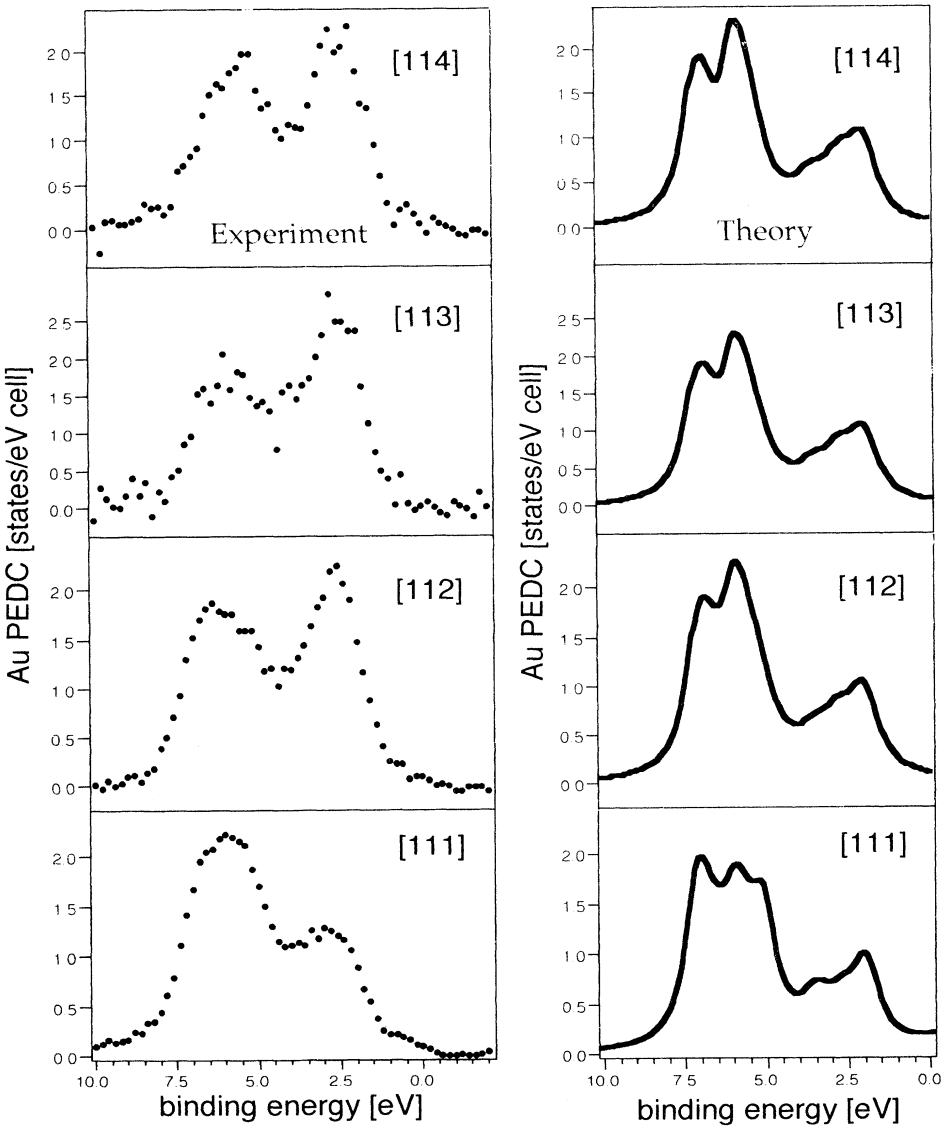

FIG. 3. The Au PEDC's analyzed along the [111], [112], [113], and [114] directions compared with theoretical PEDC's of the *d* electrons projected along the same set of directions.

in good agreement with the experiment along [111], although some hybridization above 4 eV is found in the calculations but not in the experimental data along [111]. However, this hybridization is clearly apparent in the experiments along the other three directions. Again, a smaller hybridization is predicted theoretically than is observed experimentally along the [112], [113], and [114] directions.

Eberhardt *et al.*[24] used angle-integrated photoemission at several photon energies to investigate the VB of $AuCu_3$. As discussed by Wertheim,[21] by exploiting Cooper minima near 40 and 160 eV, it is possible to obtain from these data nearly clean PEDC's of Au and Cu, respectively. Our experimental results for Cu and Au along [112], [113], and [114], which are mostly bulklike agree with the PEDC's given by Wertheim.[21] In the case of Au, both methods show the Au density of states around 2.6 eV to be higher than the density of states between 5 and 7 eV. The hybridization of Cu above 4 eV is also found in the angle-integrated measurements, although it is smaller than the one we find along [112], [113], and [114].

Because the diffraction differences get smaller from [111] to [114], the noise in the PEDC's increases towards the surface normal. As will be shown below, the small differences seen between the Au and Cu PEDC's in the [112], [113], and [114] directions are within the uncertainties of the decomposition. It can be concluded that the valence-band decomposition of $AuCu_3$ (001) yields the same results for the [112], [113], and [114] directions and, thus, the method is consistent. This agrees with the results of Heise and Courths *et al.*[6] who tried our method on TiO_2 and did not see any dependence of the PEDC's on the direction of analysis.

The main inconsistency in our data is the marked difference between the [111] and the other directions.

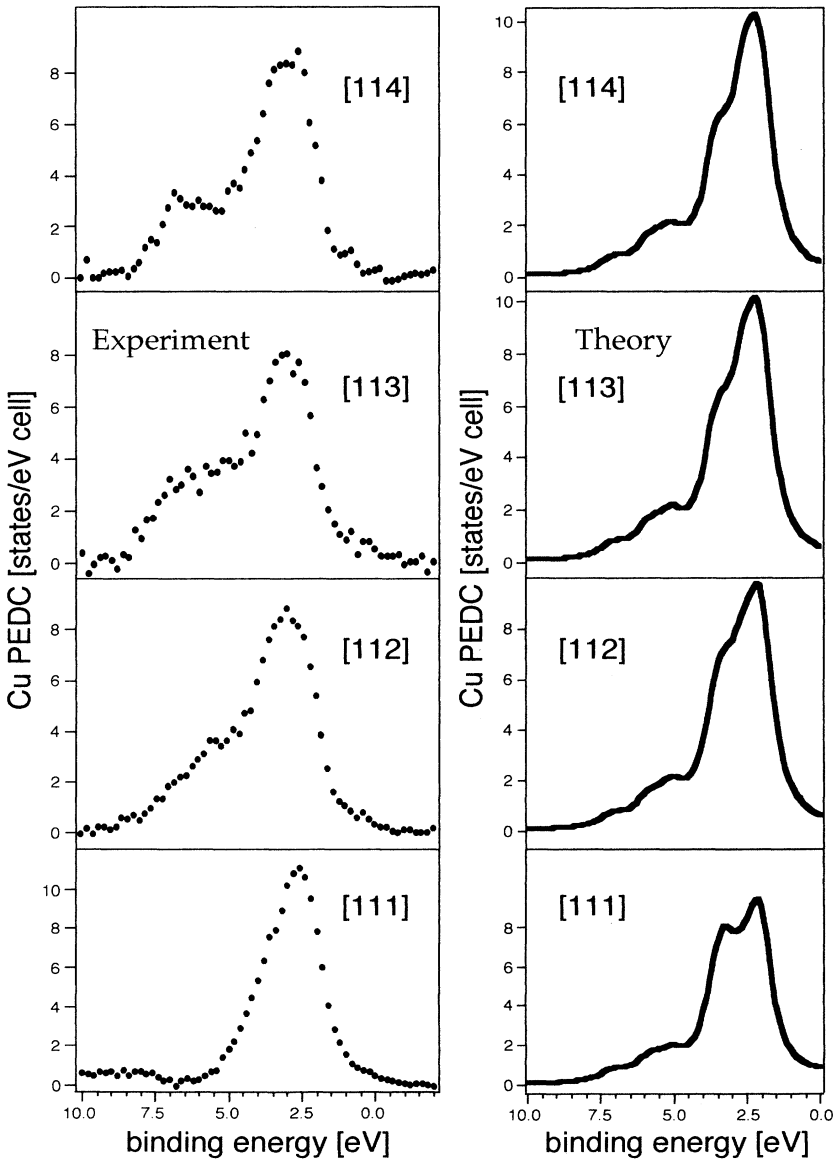

FIG. 4. The Cu PEDC's analyzed along the [111], [112], [113], and [114] direction compared with theoretical PEDC's of the *d* electrons projected along the same set of directions.

Since direct transitions will be ruled out below, two possibilities remain to explain the differences seen between the [111] and other directions. First, the emission along the [111] direction is at least 19.5° more grazing than the emission along the other three directions. Consequently, the surface contributes significantly more to the PEDC's along [111] than to the other three directions. For example, a simple model assuming isotropic damping of the electron wave in the substrate predicts about 43% of all Au electrons around 1.2 keV to be emitted from the topmost layer along [111], while it is about 32% along [112], 29% along [113], and 28% along [114]. A similar trend is predicted for Cu electrons where the corresponding percentages are roughly half what they are for Au. Although the precise numbers strongly depend on the model parameters, especially the mean-free path of the electrons inside the solid (assumed to be 12 Å for the numbers given above), the model shows that the biggest influence of the surface on the PEDC's is along [111]; the difference between the [112], [113], and [114] directions is only a few percent and can be neglected. Therefore, in agreement with our experimental results, the analysis along the [112], [113], and [114] directions should give the same PEDC's, which are most bulklike: The PEDC's along [111] will have some surface contributions in it and will be different from the other three directions. Second, in crystals with cubic symmetry, the photoemission of electrons with an initial state of e_g symmetry is suppressed along [111] and the emission from t_{2g} initial states dominates.[18] Exactly the reverse is true of the [001] direction. In the other directions, contributions from t_{2g} and e_g initial states are mixed. Because these selection rules can be derived from symmetry arguments alone, they persist even at high kinetic energies. Experimentally, such dependences have been observed in Au, although in this case the effects are smaller than those discussed here.[18] Our theoretical calculations also suggest only small differences between the e_g and t_{2g} initial states in $AuCu_3$. We, therefore, believe that surface effects are mostly responsible for the discrepancy seen in the PEDC's along [111] and the other three directions.

Historically there has been some controversy surrounding the electronic structure of ordered $AuCu_3$. Wertheim[21] argued that electrons from Au and Cu are distributed over the whole d band and that these electrons are strongly hybridized. While Sohal *et al.*[20] were only able to identify experimentally derived Au d bands at binding energies higher than 4.5 eV, their calculations show some hybridization between Au and Cu. In contrast Eberhardt *et al.*[24] concluded that the Au d states in $AuCu_3$ have an atomiclike character and are confined to binding energies above 4.5 eV. They also suggested that the Cu-d electrons change little upon alloying with Au and that no hybridization of the d bands of Au and Cu is found in $AuCu_3$. Kuhn *et al.*,[25] using the energy dependence of the photoelectron cross sections, observed that the Cu d band was narrower in $AuCu_3$ than in pure Cu and shifted towards the Fermi level, a result they interpreted as d-d repulsion between Cu and Au. However, they also found some experimental evidence of hybridization between the two elements. Very recently, Lau *et al.*[26] have measured a dispersion of the Au-like bands between 4.5- and 8-eV binding energy. Spin-resolved photoemission experiments show polarization reversal in the same region indicating a reduced spin-orbit splitting (compared to its atomic value) of about 0.8 eV.[27] It is, therefore, clear to date that a simple atomiclike picture of the Au d states is not adequate and that Au and Cu d electrons hybridize in $AuCu_3$. This is in agreement with our results, which clearly show that in $AuCu_3$ the d states of Au extend over the whole d band region and that the Cu d states are hybridized. In particular, we find for the bulklike Au PEDC's along the [112], [113], and [114] directions the Au density of states around 2.6 eV to be higher than the density of states between 5 and 7 eV.

V. STATISTICAL ERRORS

In the case of $AuCu_3$, typical differences in the diffraction patterns of two elements are of the order of 10%. Consequently, the statistical accuracy of the VB measurements must be very high, at least an order of magnitude higher than the diffraction differences, and should, thus, not exceed a few per thousand of the total signal. The total counts per channel in the VB should be of the order of 10^6 or better. Intuitively, one would expect the deconvolution of the VB to work well if the diffraction differences between the elements are large. The most favorable condition occurs near directions where the derivatives of the diffraction patterns of the two elements have opposite signs. For example, in Fig. 3 the Au signal decreases while the Cu signal increases when the direction is changed from $\phi=45°$ to $\phi=51°$. Mathematically this means that the determinant of the matrix S^{core} in Eqs. (10) and (11) is large.

In the case of an alloy with two elements, which is analyzed using two different directions, the general solution of Eqs. (10) and (11), respectively, can be written as

$$c_i=\frac{\det M_i}{\det M_0}\ , \tag{13a}$$

where

$$M_0=\begin{bmatrix} S_1^1 & S_2^1 \\ S_1^2 & S_2^2 \end{bmatrix}\ ,\quad M_1=\begin{bmatrix} I_{\text{VB}}^1 & S_2^1 \\ I_{\text{VB}}^2 & S_2^2 \end{bmatrix}\ ,$$

$$M_2=\begin{bmatrix} S_1^1 & I_{\text{VB}}^1 \\ S_1^2 & I_{\text{VB}}^2 \end{bmatrix}\ ,\quad \text{and } c_i=\frac{\sigma_i^{\text{VB}}}{\sigma_i^{\text{core}}}\frac{\mu_i^{\text{VB}}(E)}{n_i^{\text{VB}}}\ . \tag{13b}$$

Here the upper index denotes different directions (θ,ϕ), and S_i^r is the integrated core-level density of the ith element measured in direction r. I_{VB}^r is the valence-band intensity measured in direction r.

The same analysis can be done for every energy channel separately [as is assumed in Eq. (13b)] or for the energy-integrated values. In the latter case, the c^i's simply become the cross-section ratios. An upper limit for the relative error of c_i is then given by

$$\left|\frac{\Delta c_i}{c_i}\right|\le\left|\frac{\Delta\det M_i}{\det M_i}\right|+\left|\frac{\Delta\det M_0}{\det M_0}\right|\ . \tag{14}$$

The smaller the determinants of the matrices M_k are, the more difficult it is to find a unique solution for the system of Eqs. (10) and (11). All information about the PEDC is lost when $\det M_k = 0$. In that case, the system of Eqs. (10) or (11) is singular and one has measured the same information twice. Thus, the goal is to find a set of directions where all $\det M_k$'s are large. As mentioned above, one favorable configuration occurs when the derivatives with respect to the angle of the diffraction patterns of the two elements have opposite signs.

As a numerical example, the statistical errors in the case of $AuCu_3$ have been evaluated for the energy-integrated VB (i.e,the cross-section ratio) along [111]. If the measured statistical accuracies of all peaks are comparable and given by $|\Delta\alpha/\alpha|$, one finds

$$\left|\frac{\Delta c_{Cu}}{c_{Cu}}\right| \approx 25 \left|\frac{\Delta\alpha}{\alpha}\right| \quad \text{and} \quad \left|\frac{\Delta c_{Au}}{c_{Au}}\right| \approx 30 \left|\frac{\Delta\alpha}{\alpha}\right| .$$

With a total precision of all measurements of the order of one per thousand, the upper limit of the statistical error in the PEDC's is a few percent.

VI. SYSTEMATIC ERRORS

Up to this point, our analysis has been based upon Eqs. (10) and (11). These implicitly depend on the following assumptions: (i) The core-level and VB diffraction patterns of a given element at high kinetic energies are exactly equal, i.e., $g_i^{VB}(\theta,\phi) = g_i^{core}(\theta,\phi)$. (ii) Direct transitions are completely suppressed. (iii) The PEDC's are not angle dependent over the two angles considered for the deconvolutions.

In order to further elucidate the validity of these assumptions, we compare in Fig. 5 an azimuthal scan of the VB of $AuCu_3$ with a linear combination of the Au $4f$ and Cu $3p$ diffraction patterns. The coefficients of the core-level intensities were obtained by a least-square fit to the VB diffraction pattern. As a measure of the strength of the diffraction, we use the anisotropy A, defined as $A(\theta) = [I(\theta) - I_{min}]/I_{max}$. Here I_{min} and I_{max} are the minimal and maximal intensities, respectively, of one azimuthal scan and $I(\theta)$ is the intensity at a given azimuthal angle θ. The anisotropy is, thus, independent of the photon flux and the photoelectron cross sections. As expected, the two diffraction patterns are not completely equal. Differences $\Delta A = A_{VB} - A_{fit}$ of the anisotropies are typically about 2–3%. A linear regression, which correlates A_{VB} with A_{fit}, gives $A_{fit} = -0.003 + 1.01 A_{VB}$. This lies within 1% of the ideal line $A_{VB} = A_{fit}$; therefore, supporting the notion that the core-level and VB diffraction patterns of each element are essentially equal. The biggest deviations from the linear regression are found around $A \sim 15\%$ in regions where the diffraction patterns are very steep and, therefore, most sensitive to small changes in angle or energy. Such regions, which include slopes of Kikuchi bands and of forward-scattering maxima, are not well suited for the valence-band deconvolution.

In order to investigate how the deviation from the ideal linear combination affects the PEDC's, the measured VB

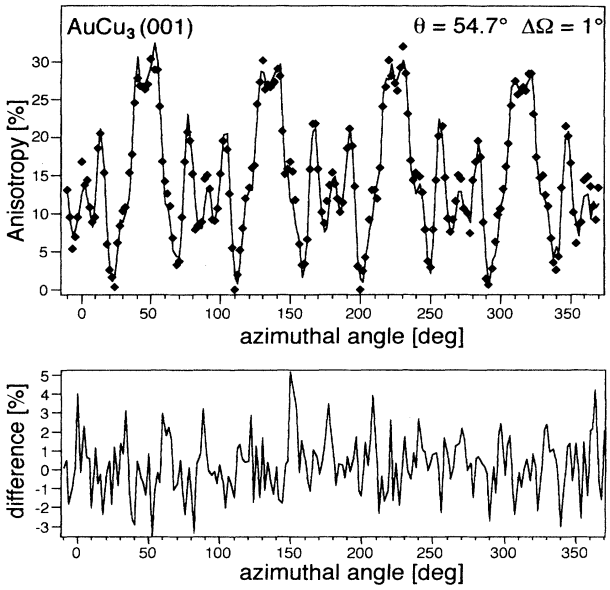

FIG. 5. Above: Comparison of the measured VB diffraction pattern (small squares) with a linear combination of the Cu $3p$ and Au $4f$ diffraction patterns. This combination (line) is a least-square fit to the VB data. Below: The difference of the anisotropies of the two diffraction patterns shown above.

intensity of $AuCu_3$ near [111] at $\phi = 51°$ (Fig. 5) was enhanced by 3% while the VB intensity at $\phi = 45°$ was left unchanged. The deconvolution of the VB into the PEDC's has then been performed. On one hand, the chosen change of 3% is of the order of the breakdown of the linear combination condition around $\phi = 45°$; on the other hand, similar differences do also exist experimentally between equal points along the four equivalent [111] directions. These experimental differences are due to crystal misalignment and crystal preparation. In Fig. 6, the resulting PEDC's are compared with the unaltered curves. As these measurements and those of Fig. 7 have been done on another sample, the results do not exactly match with the PEDC's presented before. Therefore, they show the degree of reproducibility to be expected in such studies. As shown in Fig. 7, the differences between the PEDC's obtained in this way are comparable to the differences seen between the PEDC's along the [112], [113], and [114] directions. Thus, within these limits, our method for the deconvolution of the VB yields consistent results. In contrast to the spectral shape, the cross-section ratios of each element are sensitive to changes in the integrated VB intensities. As shown in Table II, increasing the integrated VB intensity around [111] at $\phi = 51°$ by 3% will reduce the Au cross-section ratio from 0.095 to 0.067 while the Cu cross-section ratio changes from 0.51 to 0.65. If instead the integrated VB intensity at $\phi = 45°$ is increased by 3%, a Au cross-section ratio of 0.127 and a Cu cross-section ratio of 0.39 is found.

To investigate the influence of direct transitions at high kinetic energies, three sets of data measured along [111] with different angular resolution have been analyzed. By

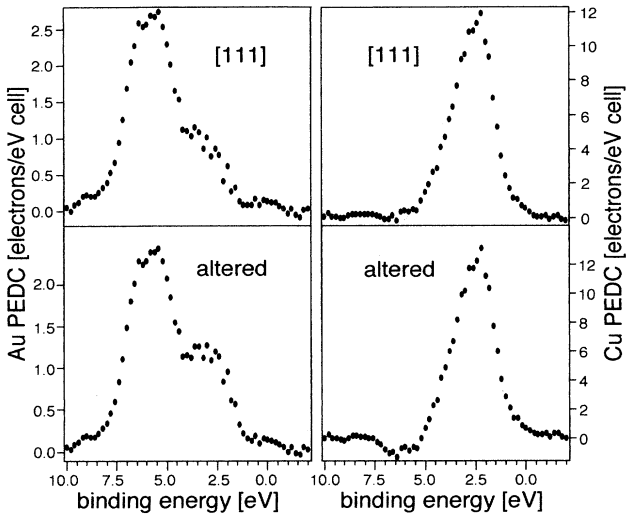

FIG. 6. Cu and Au PEDC's compared for different linear combinations of the core levels along the [111] direction. Above: Unaltered spectra, the measured intensities of the core levels and valence bands were taken for the deconvolution. Below: The measured VB spectra at $\phi=151°$ was enhanced by 3% before the deconvolution.

TABLE II. Core level to VB cross-section ratios for Au and Cu in $AuCu_3$ along the [111] direction. The deviation from the linear combination is assumed to be 3%.

Condition	$\sigma_{\text{Au VB}}/\sigma_{\text{Au }4f}$	$\sigma_{\text{Cu VB}}/\sigma_{\text{Cu }3p}$
Ratios from raw data	0.095	0.51
VB intensity at $\phi=51°$ increased by 3%	0.067	0.65
VB intensity at $\phi=45°$ increased by 3%	0.127	0.39
Mean value	0.096	0.52
Standard deviation	0.030	0.13

changing the angular resolution of the spectrometer from 1.0° to 1.6° to 2.2°, the acceptance cone projected back into the first Brillouin zone is changed from about 10° to 16° to 22° and the degree of zone averaging is changed by a factor of up to 4.8.[29] The results are presented in Fig. 7. Again, the spectra change but not significantly. Similar changes are induced by the breakdown of the linear combination condition. At a low angular resolution, the diffraction patterns lose their fine structure. Consequently, the diffraction differences between core-level intensities of the two elements are reduced and the deconvolution becomes less reliable. Confirming the initial assump-

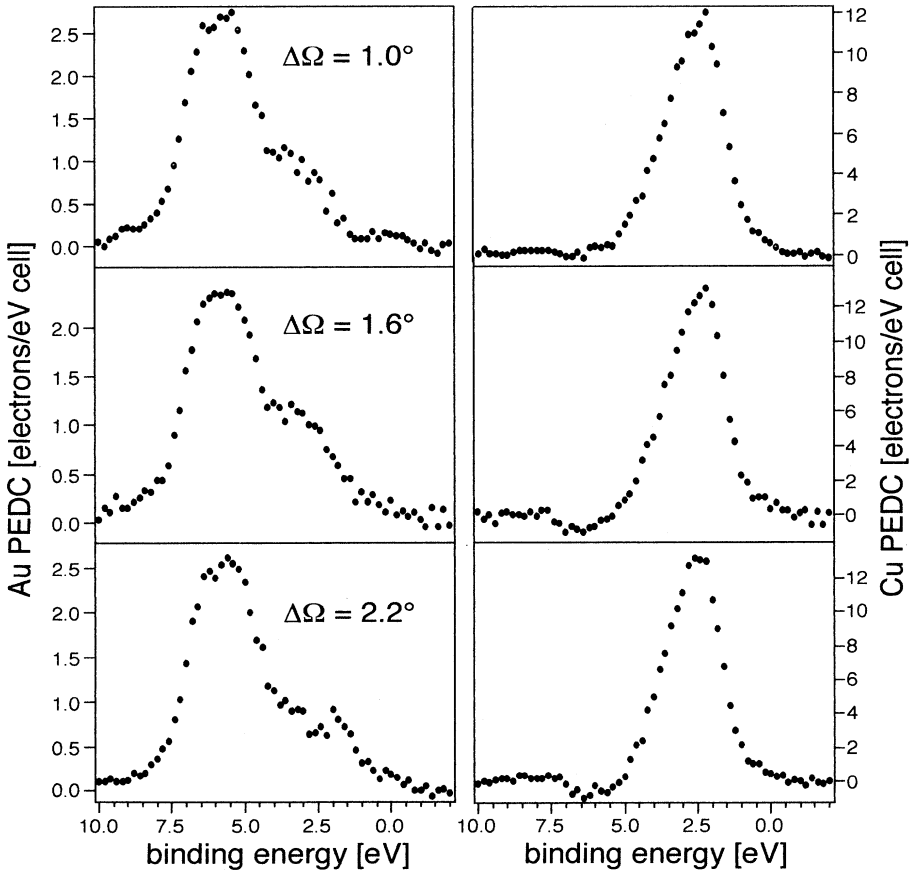

FIG. 7. Comparison of Au and Cu PEDC's of $AuCu_3$ measured with different angular resolution along [111]. The angular resolution of the full cone is indicated.

tions, it is, thus, concluded that at room temperature the deconvoluted PEDC's of $AuCu_3$ are not significantly affected by direct transitions.

Our method is, therefore, mainly limited by the residual differences between the core-level and VB diffraction patterns seen in Fig. 5. They are probably due to the different angular-momentum final states in photoemission and the small differences in the kinetic energy of the electrons. Simply increasing the measuring time to get better statistical accuracy will, therefore, not improve the reliability of the PEDC's. The diffraction differences between the elements have to be stronger than the differences seen between core-level and VB diffraction otherwise the method presented here does not work reliably and the results obtained can be erroneous.

VII. CONCLUSIONS

We have shown that in $AuCu_3$ it is possible to obtain PEDC's by exploiting differences in the photoelectron diffraction patterns. The results qualitatively reproduce the theoretical PEDC's and are in good agreement with other measurements. Experiments that exploit Cooper minima to obtain similar information have to be performed in an angle-integrated mode to sample the whole Brillouin zone at a low energy.[21,24] In contrast, our approach uses measurements with a high angular resolution. Consequently, it may be eventually possible to extend our current approach, e.g., by going to lower temperatures and using smaller angular differences in the deconvolution procedure, to examine directional dependences of the PEDC's, information that is not readily available at low kinetic energies. At energies above 1 keV, it should also be possible to measure surface PEDC's if diffraction differences at grazing angles can be found or if the surface core-level shifts can be resolved.[28,30] At high photon energies, the method is limited by a rather low energy resolution and by the fact that the valence-band intensities are only approximately a linear combination of the core-level intensities. One advantage of our method is that conventional x-ray tubes and electron spectrometers are sufficient to perform the measurements.

ACKNOWLEDGMENTS

This work was supported by the Swiss National Science Foundation. We would like to thank Thomas Straub and Professor S. Hüfner of the University of Saarbrücken for helpful discussions. One of us (A.S.) would like to thank Professor D. A. King of the University of Cambridge for his hospitality.

*Present address: Dept. of Chemistry, University of Cambridge, Lensfield Road, Cambridge CB2 1EW, England.

†Present address: Physikalisches Institut, Universität Zürich-Irchel, Winterthurerstrasse 190, 8057 Zürich, Switzerland.

[1]J. W. Cooper, Phys. Rev. **128**, 681 (1962).

[2]J. F. van Acker, P. W. J. Weijs, J. C. Fuggle, K. Horn, W. Wilke, H. Haak, H. Saalfeld, H. Kuhlenbeck, W. Braun, G. P. Williams, D. Wesner, M. Strongin, S. Krummacher, and K. H. J. Buschow, Phys. Rev. B **38**, 10 463 (1988).

[3]G. Dräger, F. Werfel, and J. A. Leiro, Phys. Rev. B **41**, 4050 (1990).

[4]A. Stuck, J. Osterwalder, T. Greber, S. Huefner, and L. Schlapbach, Phys. Rev. Lett. **65**, 3029 (1990).

[5]A. Stuck, D. Naumovic, U. Neuhaus, J. Osterwalder, and L. Schlapbach, *Synchrotron Radiation: Selected Experiments in Condensed Matter Physics,* edited by W. Czaja (Birkhaeuser-Verlag, Basel, 1991).

[6]W. Heise and R. Courths, Surf. Sci. **287/288**, 658 (1993).

[7]D. Naumovic, A. Stuck, T. Greber, J. Osterwalder, and L. Schlapbach, Phys. Rev. B **47**, 7462 (1993).

[8]J. Osterwalder, T. Greber, S. Hüfner, and L. Schlapbach, Phys. Rev. Lett. **64**, 2683 (1990).

[9]S. A. Chambers, Surf. Sci. Rep. **16**, 6 (1992).

[10]L. E. Klebanoff and D. G. Van Campen, Phys. Rev. Lett. **69**, 196 (1992).

[11]W. L. Schaich, *Photoemission in Solids I,* edited by M. Cardona and L. Ley (Springer, Berlin, 1978).

[12]N. W. Ashcroft and N. D. Mermin, *Solid State Physics* (Holt-Saunders, Tokyo, 1981).

[13]J. B. Pendry, *Low Energy Electron Diffraction* (Academic, London, 1974).

[14]N. J. Shevchik, Phys. Rev. B **16**, 3428 (1977).

[15]V. S. Sundaram, R. S. Alben, and W. D. Robertson, Surf. Sci. **46**, 653 (1974).

[16]C. S. Fadley, Prog. Surf. Sci. **16**, 275 (1984).

[17]R. J. Baird, C. S. Fadley, M. Sagurton, and Z. Hussain, Phys. Rev. B **15**, 666 (1977).

[18]D. A. Shirley, J. Stöhr, P. S. Wehner, R. S. Williams, and G. Apai, Phys. Scr. **16**, 398 (1977).

[19]P. Weinberger, A. M. Boring, R. C. Albers, and W. M. Temmerman, Phys. Rev. B **38**, 5357 (1988).

[20]G. S. Sohal, C. Carbone, E. Kisker, S. Krummacher, A. Fattah, W. Uelhoff, R. C. Albers, and P. Weinberger, Z. Phys. B **78**, 295 (1990).

[21]G. K. Wertheim, Phys. Rev. B **36**, 4432 (1987).

[22]T. M. Buck, G. H. Wheatley, and L. Marchut, Phys. Rev. Lett. **51**, 43 (1983).

[23]A. Stuck, J. Osterwalder, L. Schlapbach, and H. C. Poon, Surf. Sci. **251**, 670 (1991).

[24]W. Eberhardt, S. C. Wu, R. Garrett, D. Sondericker, and F. Jona, Phys. Rev. B **31**, 8285 (1985).

[25]M. Kuhn, T. K. Sham, J. M. Chen, and K. H. Tan, Solid State Commun. **75**, 861 (1990).

[26]M. Lau, S. Löbus, R. Courths, S. Halilov, H. Gollisch, and R. Feder, Ann. Phys. **2**, 450 (1993).

[27]C. M. Schneider, G. S. Sohal, P. Schuster, and J. Kirschner, Vacuum **41**, 511 (1990).

[28]S. B. DiCenzo, P. H. Citrin, E. Hartford, and G. K. Wertheim, Phys. Rev. B **34**, 1343 (1986).

[29]R. C. White, C. S. Fadley, M. Sagurton, and Z. Hussain, Phys. Rev. B **34**, 5226 (1986).

[30]P. H. Citrin, G.K. Wertheim, and Y. Baer, Phys. Rev. Lett. **41**, 1425 (1978).

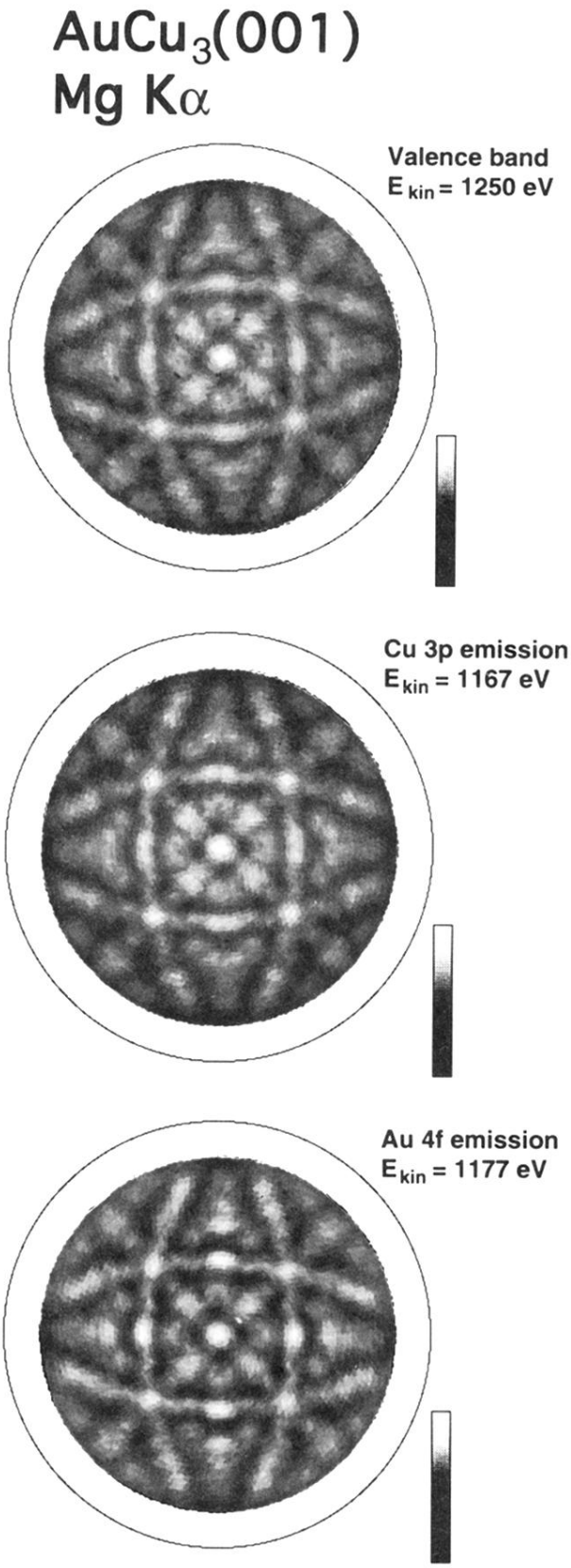

FIG. 1. Two-dimensional VB, Cu $3p$, and Au $4f$ diffraction maps of $AuCu_3$ (001) in the stereographic projection; the normal is in the center of the images while grazing incidence is marked by the circle. Along the [111], [112], [113], and [114] directions, small diffraction differences between Cu $3p$ and Au $4f$ emission can be identified.